



#### Available online at www.sciencedirect.com

### **ScienceDirect**

Acta Materialia 63 (2014) 30-43



www.elsevier.com/locate/actamat

# n-Type skutterudites $(R,Ba,Yb)_y$ Co<sub>4</sub>Sb<sub>12</sub> (R = Sr, La, Mm, DD, SrMm, SrDD) approaching $ZT \approx 2.0$

G. Rogl a,b,c,\*, A. Grytsiv A, P. Rogl N. Peranio D, E. Bauer B, M. Zehetbauer C, O. Eibl D

- <sup>a</sup> Christian Doppler Laboratory for Thermoelectric Research, Institute of Physical Chemistry, University of Vienna, Währingerstrasse 42, A-1090 Wien, Austria
  - <sup>b</sup> Christian Doppler Laboratory for Thermoelectric Research, Institute of Solid State Physics, TU-Wien, Wiedner Hauptstrasse, 8-10, A-1040 Wien, Austria

<sup>c</sup> Physics of Nanostructured Materials, University of Vienna, Boltzmanngasse 5, A-1090 Wien, Austria <sup>d</sup> Institute of Applied Physics, Eberhard Karls University of Tübingen, Auf der Morgenstelle 10, D-72076 Tübingen, Germany

Received 25 July 2013; accepted 18 September 2013 Available online 6 November 2013

#### Abstract

The influence of various fillers R (R = Sr, La, Mm, DD, SrMm, SrDD with Mm standing for mischmetal and DD for didymium) on the physical properties of the triple- and multifilled n-type skutterudites with the nominal composition ( $R_{0.33}Ba_{0.33}Yb_{0.33}Co_4Sb_{12.3}$  is investigated. In comparison to values from previous works of the authors and from the literature it is demonstrated that even small changes in the filling fractions of the fillers as well as in the total filling level influence the power factor and the thermal conductivity. These skutterudites, partially filled with multiple fillers of different chemical nature, can achieve high power factors (>6 mW m<sup>-1</sup> K<sup>-2</sup> at 823 K) and at the same time low thermal conductivity, resulting in ZT = 1.4 at 823 K. On the contrary, Yb<sub>2</sub>O<sub>3</sub> as a secondary phase in (Sr<sub>0.25</sub>Ba<sub>0.25</sub>Yb<sub>0.50</sub>)<sub>0.5</sub>Co<sub>4</sub>Sb<sub>12.5</sub> significantly reduces the thermoelectric (TE) performance due to a decreased power factor and an increased lattice thermal conductivity. However, a homogeneous nanoscale distribution of these impurities substantially improves the TE performance, resulting in ZT values of ~1.6 at 835 K. The ZT value of this skutterudite could be further enhanced to 1.9 (at 835 K) after severe plastic deformation via high-pressure torsion.

© 2013 Acta Materialia Inc. Published by Elsevier Ltd. All rights reserved.

Keywords: Skutterudites; Precipitation; High-pressure torsion; Nanomaterials

#### 1. Introduction

With respect to an increasing worldwide demand for energy, thermoelectric (TE) technology offers the possibility to convert heat, even waste heat, into useful electrical energy for various applications—cars, power plants, spacecraft, etc. [1]. In addition, TE-based heating and cooling can replace mechanical compressor-based systems and can thereby save fossil fuels and reduce greenhouse gas

emissions. The efficiency of a TE material is governed by the dimensionless TE figure of merit  $ZT = (S^2T)/(\rho\lambda)$ , where S is the Seebeck coefficient, T is the temperature,  $\rho$  is the electrical resistivity and  $\lambda$  is the thermal conductivity;  $\lambda = \lambda_e + \lambda_{ph}$ , with  $\lambda_e$  the electronic thermal conductivity and  $\lambda_{ph}$  the lattice thermal conductivity.

Skutterudites with the chemical formula  $T_4X_{12}$  (T is a transition element of the VIII group in site 8c ( ${}^{1}\!4$ , ${}^{1}\!4$ , ${}^{1}\!4$ ) and E fills the icosahedral hole in position 2a (0,0,0)) crystallize with a filled variant of the CoAs<sub>3</sub> type (LaFe<sub>4</sub>P<sub>12</sub> type, space group  $Im\overline{3}$  [2]). The physics of filled skutterudites is governed by the interplay between filler ions and their host structure [3–8]. In order to reach a maximum TE performance, the optimal filler elements, filling level and filling fraction need to be defined [9–15,6,16–21].

<sup>\*</sup> Corresponding author at: Christian Doppler Laboratory for Thermoelectric Research, Institute of Physical Chemistry, University of Vienna, Währingerstrasse 42, A-1090 Wien, Austria.

*E-mail addresses:* gerda.rogl@univie.ac.at, gerdarogl@yahoo.com (G. Rogl).

Double filling has been proved to optimize the TE properties [22–34], but in our previous investigations of n-type skutterudites [35–37] we were able to show that triple filling favourably influences the TE performance, revealing a ZT value that is obviously higher than that of double- and single-filled skutterudites, a fact also reported in other publications [38,39]. Ba and Yb have a significant mass difference, which is advantageous for lowering the lattice thermal conductivity [23,24,40,41], and therefore Ba and Yb were used in combination with other fillers, R, in triple-and multifilled skutterudites.

In the paper of Zhang et al. [35], the Yb-content of triple-filled n-type skutterudites  $(Sr_{0.1-x}Ba_xYb_{0.1})Co_4Sb_{12}$  was kept constant, whereas the two other fillers, Ba and Sr, varied; for  $Sr_{0.075}Ba_{0.025}Yb_{0.1}Co_4Sb_{12}$  a ZT > 1.4 at 800 K was gained.

The investigation of the composition dependence on the TE properties for  $(Sr_xBa_xYb_{1-2x})_yCo_4Sb_{12}$  skutterudites [37] defined a wide compositional range  $(0.25 \le x \le 0.4; 0.18 \le y \le 0.24)$ , revealing ZT > 1.4 at 800 K for  $Sr_{0.07}Ba_{0.07}Yb_{0.07}Co_4Sb_{12}$ .

Based on these results and animated by the fact that Shi et al. [39] in the series (Ba, La, Yb),  $Co_4Sb_{12}$  achieved ZT = 1.7 at 850 K for  $Ba_{0.08}La_{0.05}Yb_{0.04}Co_4Sb_{12}$ , we aim to elucidate the influence of various fillers R on the multifilled n-type skutterudites with the nominal composition ( $R_{0.33}Ba_{0.33}Yb_{0.33})_{0.35}Co_4Sb_{12.3}$  (R = Sr, La, Mm, DD, SrMm, SrDD, where Mm stands for mischmetal and DD stands for didymium).

After we had found out that R = Sr had the best TE performance, the second part of this work concerns the influence of  $Yb_2O_3$  as secondary phase in micro- and nanoscale distribution on the TE properties of  $(Sr,Ba,Yb)_yCo_4Sb_{12}$  skutterudites. In addition, the influence of the grain size on such a nanostructured material was examined.

Severe plastic deformation (SPD) is one of the ways to produce materials with ultrafine grain size. In this paper high-pressure torsion (HPT) was used, i.e. a technique based on the use of a Bridgman anvil-type device where the sample is subjected to torsional straining under a high pressure between two anvils. The advantage of HPT is that the shape of the sample remains unchanged and therefore no geometrical restriction exists on the strain and shear deformation that can be achieved via high hydrostatic pressure. In addition, hydrostatic pressure limits the extent of annihilation of deformation-induced defects, especially dislocations, and this way an enhanced formation of grain boundaries develops out of these defects with high angles of misorientation [42–46]. Therefore after HPT processing not only can crystallites smaller than about 40 nm be produced but also a high concentration of defects (mostly dislocations and vacancies) and grain boundaries are introduced [42–46], reducing the lattice thermal conductivity substantially via phonon scattering [47–50]. The fact that HPT processing of skutterudites enhances ZT is demonstrated in this work on  $Sr_{0.09}Ba_{0.11}Yb_{0.05}Co_4Sb_{12}$ , the sample with the best TE performance.

#### 2. Experimental details

The samples were prepared from Sr, Ba, La (99+ mass%, Sigma–Aldrich, Germany), Yb (99.9 mass%, Rhône-Poulenc, Shelton, CT, USA), Mm (99.9 mass% from Treibacher Industrie AG, Austria, containing 50.8% Ce, 28.1% La, 16.1% Nd, 5.0% Pr), DD (99.9 mass% from Treibacher Industrie AG, Austria, containing 4.76 mass% Pr and 95.24% Nd) and Sb ingots (99.8 mass% metals basis, Alfa Aesar, Germany), Co powder (99.9 mass%, particle size <150 μm, Sigma–Aldrich, Germany) and Co pieces (99.9 mass%, Alfa Aesar, Germany).

In a first step, precursors with compositions SrSb<sub>3</sub>, BaSb<sub>3</sub>, YbSb<sub>2</sub>, La<sub>2</sub>Co<sub>3</sub>, MmCo<sub>2</sub> and DD<sub>2</sub>Co<sub>3</sub> were prepared. Whereas SrSb<sub>3</sub>, BaSb<sub>3</sub> and YbSb<sub>2</sub> were synthesized from pieces of elements by reaction in evacuated silica tubes at 600 °C for 7 days, La<sub>2</sub>Co<sub>3</sub>, MmCo<sub>2</sub> and DD<sub>2</sub>Co<sub>3</sub> were arc-melted in Ti-gettered argon. The precursors and antimony were powdered to particle sizes below 150 μm and mixed with the Co powder to obtain a nominal composition of (R<sub>0.33</sub>Ba<sub>0.33</sub>Yb<sub>0.33</sub>)<sub>0.35</sub>Co<sub>4</sub>Sb<sub>12.3</sub> (R = Sr, La, Mm, DD, SrMm, SrDD, where SrDD and SrMm are equiatom mixtures of Sr with Mm and Sr with DD). The mixtures (total weight 10 g) were sealed in quartz tubes, heated from 550 to 950 °C at a rate of 2° min<sup>-1</sup>, reacted for 1 h, cooled to 700 °C and annealed at this temperature for 4 days.

All samples except one, further referred to as  $R = Sr_{HM}$ , which was manually ground in a tungsten carbide mortar into fine powder (<100  $\mu$ m), were ball milled in tungsten carbide vessels (volume = 80 ml, Ar filled) in a Fritsch planetary mill (Pulverisette 4) with 25 balls 10 mm in diameter for 2 h at 200 rpm (main disc) and -500 rpm (vessels). For hot pressing under argon a FCT hot-press system HP W 200/250 2200-200-KS was used with the following press conditions: 650 °C and 56 MPa (2 h). All work with powders was performed in a glovebox under Ar with less than 3 ppm  $O_2$  and 5 ppm  $H_2O$ .

X-ray powder diffraction data were obtained from a Huber Guinier powder camera and monochromatic Cu  $K_{\alpha 1}$  radiation ( $\lambda = 0.154051$  nm) with an image plate recording system. Precise lattice parameters were calculated by least-squares fits to the indexed  $2\theta$  values (calibrated with respect to Ge as internal standard;  $a_{\rm Ge} = 0.565791$  nm at room temperature) using the program STRUKTUR [51].

Quantitative Rietveld refinement was used in order to determine the total filling level,  $y_{\rm XPD}$  (occupancy of the sum of the various filler atoms in the 2a site), employing the program FULLPROF [52] by introducing the atomic ratios of the fillers from the electron probe microanalyses,  $y_{\rm EPMA}$  (EPMA, energy dispersive X-ray spectroscopy (EDX) with an INCA Penta FETx3 in a Zeiss SUPRA55VP equipment).

Specimens were cut in plan-view for investigations by analytical transmission electron microscopy (TEM). Samples were prepared as explained in more detail in Refs. [53,54]. For ion etching of the specimens a Fischione

1010 ion mill was used. For the TEM analysis, a Zeiss 912 Omega was used, operated at 120 kV and equipped with an omega energy filter and an EDX detector. Energy-filtered bright-field and dark-field images were acquired under defined diffraction conditions (with strongly excited reflections) for imaging grain boundaries and dislocations. Selected-area electron diffraction patterns were achieved using an aperture to select areas for diffraction of 750 nm in size. Superimposed energy-filtered images (RGB) were acquired for the imaging of the secondary phases using energy losses of 17, 31 and 59 eV and a slit aperture of 10 eV width. Point EDX spectra were achieved with a spot size of 32 nm. Details of the quantitative chemical analysis by EDX are explained elsewhere [54].

The resistivity and Seebeck coefficient above room temperature were measured simultaneously with an ULVAC-ZEM3 (Riko, Japan) system. The thermal conductivity above room temperature was calculated from the thermal diffusivity  $D_t$  measured by a flash method (Flashline-3000, ANTER, USA), specific heat  $C_p$  and density  $d_m$  using the relationship  $\lambda = D_t C_p d_m$ . Measurement errors for the electrical resistivity and Seebeck measurements are <2% and <3%, for thermal conductivity  $\sim5\%$ , which all are in the range confirmed from parallel measurements in another laboratory [55].

Hall effect and the electrical resistivity at room temperature were measured with an in-house-constructed system based on the van der Pauw method. Disks with a diameter of 10 mm and height of 1 mm were used for this measurement at 0.65 T.

The density  $(d_m)$  of each sample was obtained by the Archimedes method, using distilled water. The relative densities  $(d_r)$  (in%) were calculated with respect to the X-ray density  $d_X = (MZ)/(VN)$ , where M is the molar mass, Z is the number of formula units per cell, N is Loschmidt's number and V is the volume of the unit cell.

After the first series of samples (set 1) was investigated, a second series of samples (set 2) was prepared (details of the sample preparation are given in Section 4.1) to further improve the physical properties by a nanoscale distribution of impurities.

The sample with the highest ZT was HPT processed. For this task two discs with a diameter of 10 mm and a thickness of  $\sim$ 1 mm were cut from the hot-pressed cylindrical samples and plastically deformed with a special facility constructed by W. Klement, Austria under the following processing conditions: 4 GPa pressure, 1 revolution, room temperature (for details of HPT processing of skutterudites, see Refs. [56,57]). As the shear strain  $\gamma$  of HPT-processed samples is dependent on the number of revolutions, n, the radius, r, and the thickness, t, of the sample disc  $(\gamma = 2\pi nr/t)$ , the sample after HPT processing is not homogeneous with respect to the crystallite size and defects because the shear strain decreases from the rim towards the center of the processed disc. Recently [58] it was shown that the center of the sample could also be sheared due to a parallel shift of the axes of the upper and lower anvil. For

the measurement of the thermal conductivity a disc with a diameter of 6 mm was cut ultrasonically from the processed disc, covering the inner, less deformed part. For the measurements of electrical resistivity and Seebeck coefficient a cuboid was cut from the middle and rim part of the processed disc.

## 3. Results and discussions for set 1, the series with the nominal composition $(R_{0.33}Ba_{0.33}Yb_{0.33})_{0.35}Co_4Sb_{12.3}$ (R = Sr, La, Mm, DD, SrMm, SrDD)

#### 3.1. Structural characterization

The X-ray intensity patterns of all skutterudites (R<sub>0.33</sub>- $Ba_{0.33}Yb_{0.33})_{0.35}Co_4Sb_{12.3}$  (R = Sr, La, Mm, DD, SrMm, SrDD) were completely indexed on the base of a body-centered cubic lattice, suggesting isotypism with the ordered LaFe<sub>4</sub>P<sub>12</sub>-type. Taking the full occupancies of Co in 8c and Sb in 24 g from EPMA data, the total occupancy of the R atoms in position 2a (0,0,0) was refined by introducing the atomic ratios of the filler atom species as determined by EPMA. The R contents based on this procedure  $(y_{R,EPMA})$  are listed in Table 1. Normalized to 4 Co atoms, in all cases 12.1(1) Sb atoms per formula unit were found. It turned out that all Sr atoms entered the skutterudite cage but not all of the La, Yb, DD and Mm atoms, which formed secondary phases, LaSb<sub>2</sub>, YbSb<sub>2</sub>, DDSb<sub>2</sub> and MmSb<sub>2</sub>, respectively. These secondary phases remained even after annealing the samples at 800 °C for 1 week.

The grain sizes of the BM samples determined by TEM investigations are  $\sim 1.1~\mu m$ . The crystallite size of the particles obtained from scanning electron microscopy (SEM) images is in the range 100–300 nm; for the HM sample (R = Sr<sub>HM</sub>), however, the crystallite size is about 100 times larger and about 10  $\mu m$ . These crystallite sizes agree well with the data from our previous works [33,34,47,59,57,60].

The relative density  $d_r$  for all samples is  $\geq 98.6\%$ , including the manually ground sample.

#### 3.2. Physical properties

Room-temperature TE properties as well as the maximum ZTs at the corresponding temperatures of all triple and multifilled skutterudites studied in this paper are shown in Table 2 in comparison with literature data. The electrical resistivity (Fig. 1, Table 2), increases with increasing temperature for all samples, indicating that they are heavily doped semiconductors. All resistivity values at about 823 K are below 800  $\mu\Omega$  cm, at room temperature in the range of 300–420  $\mu\Omega$  cm and therefore in the same range as reported for  $Ba_{\nu}La_{\nu}Yb_{\nu}Co_{4}Sb_{12}$  [39]. The samples of the  $(Sr_{x}Ba_{x}Yb_{1-2x})_{\nu}Co_{4}Sb_{12}$  series of a previous work [37] had higher resistivities at room temperature as well as at 823 K.

As expected for filled Co<sub>4</sub>Sb<sub>12</sub>-skutterudites, their Seebeck coefficients (Fig. 2) are negative, due to the fact that the fillers are n-type dopants for CoSb<sub>3</sub>. The absolute

Table 1 Data for multifilled n-type skutterudites: filler, R, filling level of each individual R, total filling level from EPMA ( $y_{\text{EPMA}}$  total, referring to formula normalized to 4 Co atoms), lattice parameter (a in nm).

	R		y <sub>EPMA</sub> total	а				
	Sr	Ba	La	Mm	DD	Yb		
Set 1								
Sr	0.08(3)	0.11(5)	_	_	_	0.04(3)	0.23(9)	0.90623(1)
$Sr_{HM}$	0.13(4)	0.21(7)	_	_	_	0.04(2)	0.38(8)	0.90687(3)
La	-	0.13(7)	0.02(1)	_	_	0.04(3)	0.19(6)	0.90592(3)
Mm	_	0.13(4)	_	0.06(4)	_	0.01(1)	0.20(7)	0.90565(1)
DD	_	0.12(5)	_		0.06(4)	0.02(2)	0.19(4)	0.90563(1)
SrMm	0.04(5)	0.11(5)	_	0.04(3)	_	0.02(2)	0.21(7)	0.90595(2)
SrDD	0.01(1)	0.15(7)	_	-	0.03(3)	0.03(1)	0.22(6)	0.90588(3)
Set 2, $R = Sr$								
Sr(S)	0.10(2)	0.12(2)				0.04(2)	0.26(3)	0.90605(2)
Sr(A)	0.09(2)	0.11(2)	_	_	_	0.05(2)	0.25(5)	0.90581(2)
After HPT	. ,	. ,				. ,	` '	0.90599(3)
After heating								0.90590(1)
Sr <sub>HM</sub> (B)	0.08(2)	0.12(1)	_	_	_	0.06(4)	0.26(6)	0.90594(1)
Sr(C) (80%A + 20%B)	0.08(2)	0.10(2)	_	_		0.06(2)	0.24(3)	0.9604(1)
Sr(D) (60%A + 40%B)	0.07(3)	0.10(5)	_	_	_	0.06(2)	0.23(7)	0.90636(4)

Table 2 Room temperature measured density,  $d_m$  (g/cm<sup>3</sup>), electrical resistivity,  $\rho$  (μΩ cm), Seebeck coefficient, S (μV K<sup>-1</sup>), power factor, pf (mW/cm K<sup>2</sup>), thermal conductivity,  $\lambda$ , and lattice thermal conductivity,  $\lambda_{ph}$  (mW/cm K), ZT as well as max. ZT, calculated/measured electron carrier density, n (×10<sup>20</sup> cm<sup>-3</sup>).

	$d_m$	$\rho$	S	pf	λ	$\lambda_{ph}$	ZT	$ZT_{823K}$	n cal.	n meas.	Refs.
Samples set 1 with the composition	on (nominal	$(R_{0.33}E)$	$Ba_{0.33}Yb_{0.33}$	<sub>0.35</sub> Co <sub>4</sub> Sb	12.3						
R = Sr	7.69	305	-110	4.0	32	5.8	0.4	1.4	7.0	_	_a
$R = Sr_{HM}$	7.61	327	-110	3.7	36	12.2	0.3	1.1	6.8	_	_a
R = La	7.68	376	-115	3.5	33	10.6	0.3	1.2	6.2	_	_a
R = Mm	7.69	392	-113	3.3	34	11.9	0.3	1.2	5.8	_	_a
R = DD	7.67	429	-128	3.8	33	13.9	0.4	1.0	5.8	_	_a
R = SrMm	7.65	355	-111	3.5	30	8.3	0.4	1.3	6.6	_	_a
R = SrDD	7.65	344	-109	3.5	31	7.8	0.3	1.3	6.7	_	_a
		$\rho$	S	pf	λ	$\lambda_{ph}$	ZT	$ZT_{835K}$			Refs.
Samples set 2 with the composition	on (nominal	$(R_{0.25}E)$	$Ba_{0.25}Yb_{0.5})_0$	.5Co <sub>4</sub> Sb <sub>12</sub>	.5						
R = Sr(S)	7.62	404	-120	3.6	38	17.6	0.5	1.2	5.7	_	_a
R = Sr(A)	7.68	351	-122	4.2	29	5.0	0.8	1.6	6.7	6.8	_a
R = Sr(A), after HPT, T incr.	7.30	791	-121	1.9	16	4.5	0.7	1.9	6.4	_	_a
R = Sr(A), after HPT, T decr.	7.30	630	-120	2.3	18	3.6	0.7	1.7	6.5	_	_a
$R = Sr_{HM}(B)$	7.67	354	-118	3.9	30	6.6	0.7	1.5	6.5	_	_a
R = Sr (C: 80%A + 20%B)	7.69	370	-122	4.0	30	7.3	0.7	1.5	5.6	_	_a
R = Sr (D: 60%A + 40%B)	7.69	367	-117	3.7	31	6.7	0.7	1.6	5.4	_	_a
		$\rho$	S	pf	λ	$\lambda_{ph}$	ZT	$ZT_{800K}$			Refs.
Composition $(Sr_xBa_xYb_{1-2x})_yCo$	$_{4}Sb_{12}$	<u>-</u>							<u></u>		
$Sr_{0.03}Ba_{0.03}Yb_{0.1}Co_4Sb_{12}$	7.70	612	-138	3.1	27	17	0.35	1.3	3.5	5.1	[37]
$Sr_{0.07}Ba_{0.07}Yb_{0.07}Co_4Sb_{12}$	7.58	595	-140	3.3	23	13	0.43	1.4	4.1	5.6	[37]
$Sr_{0.1}Ba_{0.1}Yb_{0.03}Co_4Sb_{12}$	7.70	486	-118	2.9	20	6	0.44	1.4	7.5	6.1	[37]
		$\rho$	S	pf	λ	$\lambda_{ph}$	ZT	$\mathrm{ZT}_{800\mathrm{K}}$			Refs.
Composition $(Sr_{0,1-x}Ba_xYb_{0,1})$ Composition	$o_{A}Sb_{12}$										
Sr <sub>0.025</sub> Ba <sub>0.075</sub> Yb <sub>0.1</sub> Co <sub>4</sub> Sb <sub>12</sub>	7.70	300	-118	4.6	33	7	0.42	1.3	1.42	_	[35]
Sr <sub>0.05</sub> Ba <sub>0.05</sub> Yb <sub>0.1</sub> Co <sub>4</sub> Sb <sub>12</sub>	7.72	300	-117	4.6	31	8	0.45	1.3	1.41	_	[35]
$Sr_{0.075}Ba_{0.025}Yb_{0.1}Co_4Sb_{12}$	7.73	300	-115	4.4	29	5	0.46	1.4	1.54	-	[35]
		$\rho$	S	pf	λ	$\lambda_{ph}$	ZT	$ZT_{850K}$			Refs.
Composition (Ba, La, Yb) <sub>v</sub> Co <sub>4</sub> Sb	12										
$Ba_{0.06}La_{0.05}Yb_{0.02}Co_4Sb_{12}$	7.38	546	-138	3.5	30	16.5	0.35	1.4	_	2.39	[39]
Ba <sub>0.08</sub> La <sub>0.05</sub> Yb <sub>0.04</sub> Co <sub>4</sub> Sb <sub>12</sub>	7.38	417	-126	3.8	27	9.4	0.42	1.7	_	3.66	[39]
Ba <sub>0.010</sub> La <sub>0.05</sub> Yb <sub>0.07</sub> Co <sub>4</sub> Sb <sub>12</sub>	7.63	333	-107	3.4	31	8.9	0.33	1.6	_	4.95	[39]
Ba <sub>0.09</sub> La <sub>0.04</sub> Yb <sub>0.13</sub> Co <sub>4</sub> Sb <sub>12</sub>	7.67	327	-104	3.3	30	7.5	0.33	1.4	_	5.52	[39]
$Ba_{0.09}La_{0.04}Yb_{0.14}Co_4Sb_{12}$	7.53	297	-93	2.9	30	5.3	0.29	1.3	-	7.64	[39]

<sup>&</sup>lt;sup>a</sup> This work.

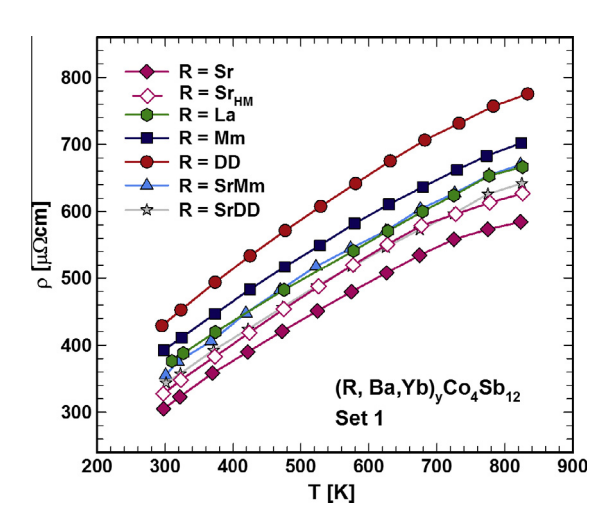


Fig. 1. Samples of set 1: electrical resistivity,  $\rho$ , vs. temperature of  $(R,Ba,Yb)_{\nu}Co_4Sb_{12}$   $(R=Sr,Sr_{HM},La,DD,MM,SrMm,SrDD)$ .

values of all Seebeck coefficients increase nearly linearly with increasing temperature with values close to each other, reaching values of -181 to  $-192\,\mu\text{V K}^{-1}$  at high temperatures, as high or even higher than values reported in the literature [35,37,39]. All Seebeck data are very close to each other and in line with the electrical resistivity: the skutterudite with the highest resistivity also has the highest absolute value of the Seebeck coefficient, and the one with the lowest resistivity has the lowest absolute value of the Seebeck coefficient; this trend also applies to the microstructured sample,  $R = Sr_{HM}$ .

From an almost linearly varying S(T) one can extract the charge carrier density, n, employing Mott's formula:

$$S = \frac{\pi^2 k_B^2 2m_e}{|e|\hbar^2 (3n\pi^2)^{2/3}} T,\tag{1}$$

with  $|e| = 1.6022 \times 10^{-19}$  As,  $k_B = 1.3807 \times 10^{-23}$  J K<sup>-1</sup>,  $\hbar = 1.0546 \times 10^{-34}$  m<sup>2</sup> s<sup>-1</sup> kg and  $m_e = 9.1094 \times 10^{-31}$  kg. The electron carrier density, in the range of

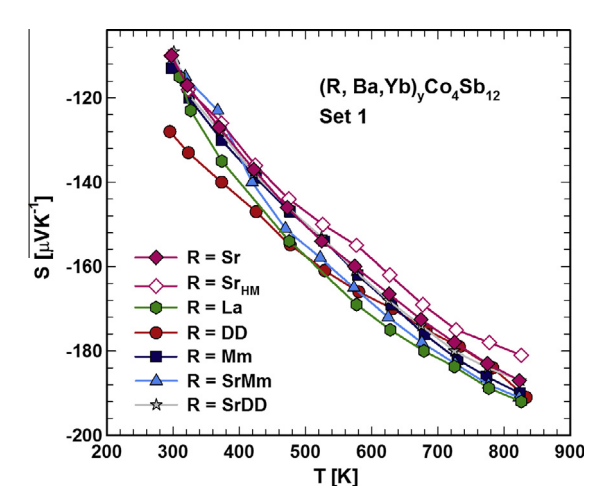


Fig. 2. Samples of set 1: Seebeck coefficient, S, vs. temperature of  $(R,Ba,Yb)_{\nu}Co_4Sb_{12}$  ( $R=Sr,Sr_{HM},La,DD,MM,SrMm,SrDD$ ).

 $n=5.8\times10^{20}$ – $7.0\times10^{20}\,\mathrm{cm^{-3}}$  (for details see Table 1), was calculated for the temperature region from 300 to 400 K. Generally n did not vary much; however, the sample with  $R=\mathrm{Sr}$  with the lowest electrical resistivity has the highest n. and the samples with  $R=\mathrm{DD}$  and  $R=\mathrm{Mm}$  with high electrical resistivities have the lowest electron carrier densities, indicating that the more charge carriers there are, the higher the electrical conductivity. As the fillers are effective n-type dopants for  $\mathrm{CoSb}_3$ , the carrier concentration must increase with increasing total filling level. This is true for the investigated skutterudites ( $R_{0.33}\mathrm{Ba}_{0.33}$ - $\mathrm{Yb}_{0.33}$ ) $_{0.35}\mathrm{Co}_4\mathrm{Sb}_{12.3}$  even though the fillers are different. Quantitatively, the charge carrier concentration can be derived from the Hall coefficient  $R_H$  via:

$$n = f/(R_H e), \tag{2}$$

where e is the elementary charge and f is a parameter that depends on the temperature, the scattering mechanism of the charge carriers and the Fermi level. For degenerate systems f does not vary much (<10%) from unity and therefore f was assumed to be 1.

For all samples the  $R_H$  values are negative, consistent with the negative Seebeck coefficient, and are around 0.001 cm<sup>3</sup> C<sup>-1</sup> at room temperature. The room-temperature Hall mobility,  $\mu$ , was estimated from:

$$\mu = 1/(\rho_{ne}). \tag{3}$$

The mobility,  $\mu \approx 27 \text{ cm}^2 \text{ V}^{-1} \text{ s}^{-1}$ , is almost sample independent and fits well to data from the literature [36,37,39].

All samples (Figs. 3 and 6) have very high power factors, >5 mW cm<sup>-1</sup> K<sup>-2</sup> at 823 K and even the sample with the lowest power factor (R = DD) achieves almost this value. The highest power factor is observed for R = Sr with 6.0 mW m<sup>-1</sup> K<sup>-2</sup> at 823 K, topping most of the best values of single-, double- and multifilled skutterudites [12,15,6,16,18–21,33,34,37,39], e.g. Ba<sub>0.08</sub>La<sub>0.05</sub>Yb<sub>0.04</sub>Co<sub>4</sub>Sb<sub>12</sub> [39] which has a power factor of  $\sim$ 5.5 mW m<sup>-1</sup> K<sup>-2</sup>

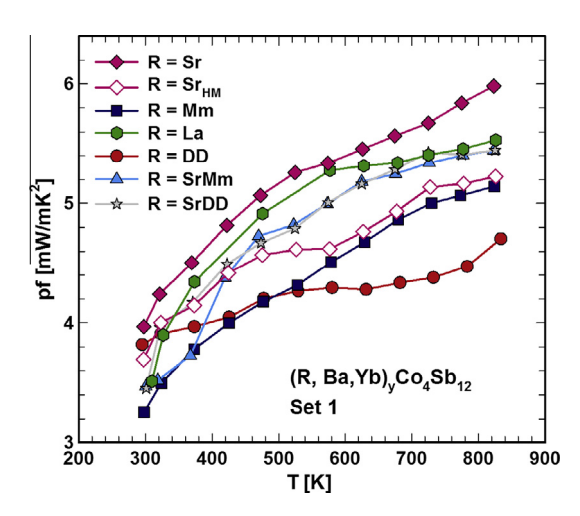


Fig. 3. Samples of set 1: power factor vs. temperature of  $(R,Ba,Yb)_yCo_4$ .  $Sb_{12}$   $(R = Sr, Sr_{HM}, La, DD, MM, SrMm, SrDD)$ .

at 823 K (see also Fig. 6). These high power factors agree well with the calculations done in recent papers by Shi et al. [24,39], which reported that the optimum carrier density for partially filled skutterudites should be between  $6 \times 10^{20}$  and  $12 \times 10^{20}$  cm<sup>-3</sup>. For the multifilled skutterudites with R = SrMm and SrDD the power factors are between those of R = Sr and R = Mm and R = Sr and R = DD, respectively.

The total thermal conductivity and its phonon component are displayed in Fig. 4 for the temperature range 400-823 K. All samples have very similar thermal conductivity values  $31 \le \lambda \le 38 \text{ mW cm}^{-1} \text{ K}^{-1}$  in this temperature range, increasing only very slowly with increasing temperature. No distinct dependence on the fillers R could be detected, though for the microstructured sample  $(R = Sr_{HM})$  higher  $\lambda$ -values were observed below 600 K. All thermal conductivity values of this series of skutterudites (set 1) are slightly higher than those reported for the Ba<sub>u</sub>La<sub>v</sub>Yb<sub>w</sub>Co<sub>4</sub>Sb<sub>12</sub> series with triple-filled  $25 < \lambda < 35 \text{ mW cm}^{-1} \text{ K}^{-1}$  [39] (see also Fig. 6 and Table 2) or  $(Sr_xBa_xYb_{1-2x})_vCo_4Sb_{12}$  [37], but are in the same range as found for the series (Sr,Ba,Yb), Co<sub>4</sub>Sb<sub>12</sub> reported by Zhang et al. [35]. The lattice thermal conductivity,  $\lambda_{ph}$ , was obtained by subtracting the electronic contribution  $\lambda_e$ , from the total thermal conductivity  $\lambda$ assuming the validity of the Wiedemann-Franz law,  $\lambda_e \approx L_0 T/\rho$  with the Lorenz number  $L_0 = 2.45 \times 10^{-8}$  $W \Omega K^{-2}$ . As can be seen in the lower part of Fig. 4,  $\lambda_{ph}$  slightly decreases with increasing temperature. In our recent investigation [37] we used the method of Cahill and Pohl [61] and calculated the minimum thermal conductivity  $\lambda_{\min} = 6.4 \text{ mW cm}^{-1} \text{ K}^{-1}$  at room temperature for  $Sr_{0.07}Ba_{0.07}Yb_{0.07}Co_4Sb_{12}$ . This value is higher than  $\lambda_{\min} = 5.2 \text{ mW cm}^{-1} \text{ K}^{-1}$  reported by Shi et al. [39] for his multifilled skutterudites but close to the lattice thermal conductivity in our series.

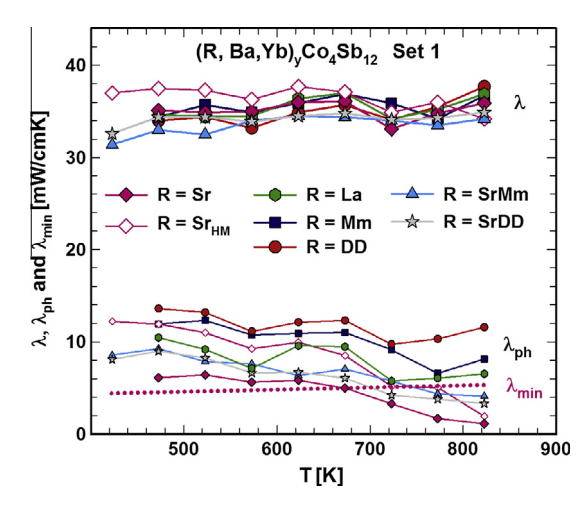


Fig. 4. Samples of set 1: thermal conductivity,  $\lambda$ , and lattice thermal conductivity,  $\lambda_{ph}$ , vs. temperature of  $(R,Ba,Yb)_yCo_4Sb_{12}$   $(R=Sr,Sr_{HM},La,DD,MM,SrMm,SrDD)$ . Dotted line:  $\lambda_{min}$  for  $Sr_{0.07}Ba_{0.07}Yb_{0.07}Co_4Sb_{12}$  [37].

It was recently reported [23,39] that it is useful to optimize the filling fractions with various charge states in order to obtain the optimum carrier concentration range for high power factors and at the same time to combine fillers with different vibrational frequencies to achieve a broad spectrum scattering for low thermal conductivity. Double-filled skutterudites with Ba and Yb as fillers, which have significantly different atomic resonances, fulfill these conditions [24]. It was calculated that for triple-filled n-type skutterudites, Ba, La and Yb should be the ideal combination because the vibrational frequency of La is between those of Ba and Yb [39], and the experimental proof was the very low  $\lambda_{ph}$  achieved for the Ba<sub>u</sub>La<sub>v</sub>Yb<sub>w</sub>Co<sub>4</sub>Sb<sub>12</sub> series (see also Table 2). In this work we combined Ba and Yb not only with La but also with Sr, DD, Mm, and SrMm and SrDD. Of course in the Ba<sub>u</sub>La<sub>v</sub>Yb<sub>w</sub>Co<sub>4</sub>Sb<sub>12</sub> series the total filling level and the ratio of the fillers was not exactly the same as in the (R,Ba,Yb), Co<sub>4</sub>Sb<sub>12</sub> series discussed here, and therefore a one-to-one comparison is not possible; however, we observed the lowest  $\lambda_{ph}$  for the combination (Sr, Ba, Yb),  $Co_4Sb_{12}$ .

The temperature dependence of ZT is shown in Fig. 5. At 823 K (see also Fig. 6b) all samples of the (R, Ba, Yb)<sub>y</sub>Co<sub>4</sub>. Sb<sub>12</sub> series have ZT > 1; the skutterudites with R = Sr have the highest value ZT > 1.4, followed by R = SrMm and R = SrDD with ZT  $\approx$  1.3 and R = La with ZT = 1.2 (Table 2). For this series of skutterudites R = Sr or Sr in combination with Mm and DD showed the best TE performance.

For the practical use of these materials as legs of TE modules, not only the ZT value at a certain temperature is important, but in addition the so-called thermal–electric conversion efficiency  $\eta$  (in%) for the material should be as high as possible over a wide temperature range. The thermal–electric conversion efficiency  $\eta$  is calculated from the expression:

$$\eta = \frac{T_h - T_c}{T_h} \frac{\sqrt{1 + (ZT)_a} - 1}{\sqrt{1 + (ZT)_a} + \frac{T_c}{T_c}},\tag{4}$$

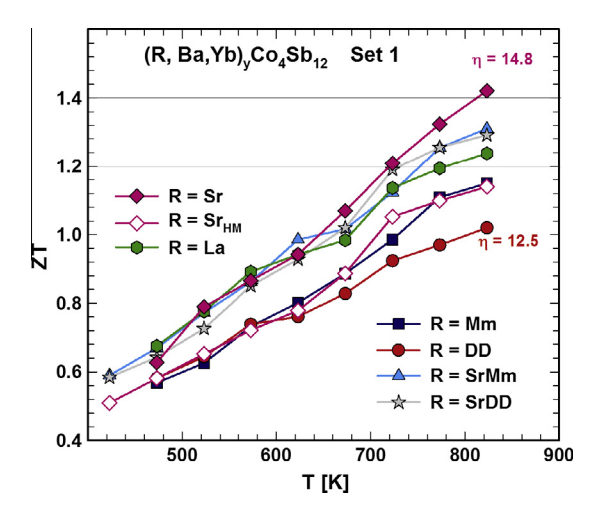


Fig. 5. Samples of set 1: figure of merit, ZT, vs. temperature of  $(R,Ba,Yb)_{\nu}Co_4Sb_{12}$   $(R=Sr,Sr_{HM},La,DD,MM,SrMm,SrDD)$ .

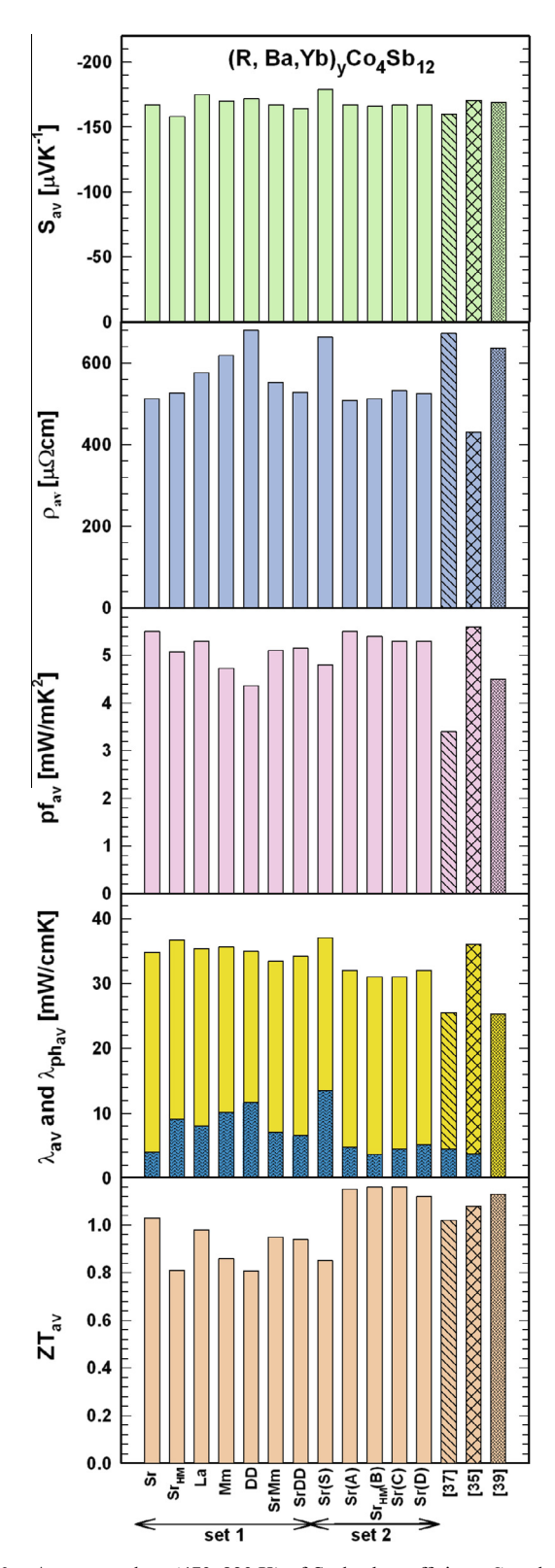


Fig. 6a. Average values (473–823 K) of Seebeck coefficient,  $S_{av}$ , electrical resistivity,  $\rho_{av}$ , power factor,  $pf_{av}$ , thermal and lattice thermal conductivity,  $\lambda_{av}$ ,  $\lambda_{phav}$ , figure of merit, ZT<sub>av</sub>, of samples (R,Ba,Yb)Co<sub>4</sub>Sb<sub>12</sub> of set 1 (R = Sr, Sr<sub>HM</sub>, La, DD, Mm, SrMm, SrDD) and of set 2 (R = Sr(A), Sr<sub>HM</sub>(B), Sr(C), Sr(D)) in comparison to Sr<sub>0.07</sub>Ba<sub>0.07</sub>Yb<sub>0.07</sub>Co<sub>4</sub>Sb<sub>12</sub> [37], Sr<sub>0.075</sub>Ba<sub>0.025</sub>Yb<sub>0.1</sub>Co<sub>4</sub>Sb<sub>12</sub> [35] and Ba<sub>0.08</sub>La<sub>0.05</sub>Yb<sub>0.04</sub>Co<sub>4</sub>Sb<sub>12</sub> [39].

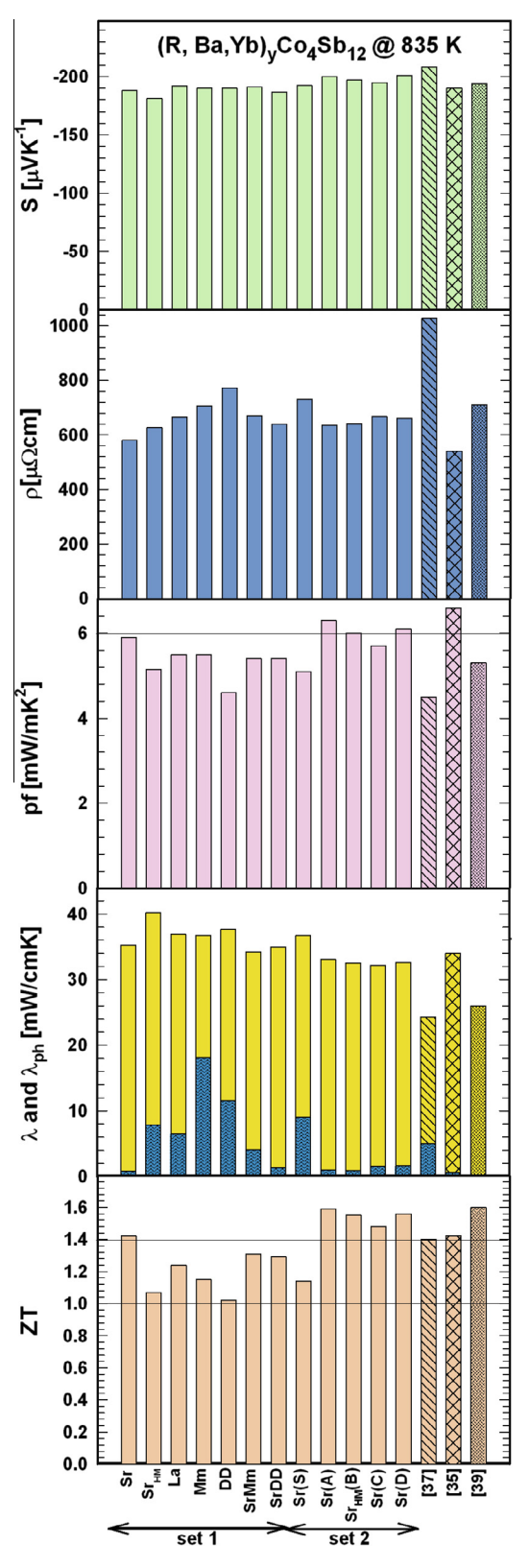


Fig. 6b. Seebeck coefficient, S, electrical resistivity,  $\rho$ , power factor, pf, thermal conductivity,  $\lambda$ , figure of merit, ZT, at 835 K of samples (R,Ba,Yb)Co<sub>4</sub>Sb<sub>12</sub> of set 1 (R = Sr, Sr<sub>HM</sub>, La, DD, Mm, SrMm, SrDD) and of set 2 (R = Sr(A), Sr<sub>HM</sub>(B), Sr(C), Sr(D)) in comparison to Sr<sub>0.07</sub>Ba<sub>0.02</sub>Yb<sub>0.07</sub>Co<sub>4</sub>Sb<sub>12</sub> [37], Sr<sub>0.075</sub>Ba<sub>0.025</sub>Yb<sub>0.1</sub>Co<sub>4</sub>Sb<sub>12</sub> [35] and Ba<sub>0.08</sub>La<sub>0.05</sub>Yb<sub>0.04</sub>Co<sub>4</sub>Sb<sub>12</sub> [39].

including the Carnot efficiency (where  $T_h$  and  $T_c$  are the temperatures on the hot (800 K) and the cold (300 K) side, respectively) as well as (ZT)<sub>a</sub>, which is the average value between  $T_c$  and  $T_h$ . For all samples 12.5%  $\leq \eta \leq$  14.8% with the highest value,  $\eta = 14.8\%$ , for Sr<sub>0.06</sub>Ba<sub>0.09</sub>Yb<sub>0.03</sub>Co<sub>4</sub>Sb<sub>12</sub> (R = Sr). The latter exhibits the highest average ZT and the highest ZT = 1.43 at 823 K.

Comparing the average values of the physical properties with respect to the filler R, it is obvious from Fig. 6a that the thermal conductivity for all samples is about the same with a slightly higher value for the microstructured skutterudites. The phonon component of the thermal conductivity of this investigation has the lowest average value for R = Sr. The Seebeck coefficient has the highest average value for R = La; however, due to the higher average electrical resistivity, the power factor is only second best after the average power factor for  $R = Sr (pf_{av} > 5 \text{ mW m}^{-1})$ K<sup>-2</sup>). This high power factor plays an important role in the skutterudite with R = Sr having the highest ZT value. The highest average ZT values belong to all three samples with Sr, i.e. R = Sr, SrMm and SrDD, whereas the lowest value has the sample with the micro grain size,  $R = Sr_{HM}$ , followed by the sample with R = DD, which shows the highest average resistivity in this series.

In Fig. 6b all physical properties at 823 K of this series of skutterudites are displayed in comparison with literature data [35,37,39]. The highest Seebeck coefficient, and in parallel the highest electrical resistivity and the lowest thermal conductivity, was obtained for Sr<sub>0.07</sub>Ba<sub>0.07</sub>Yb<sub>0.07</sub>Co<sub>4</sub>Sb<sub>12</sub> [37]. An outstanding low electrical resistivity and therefore the highest power factor can be seen for  $Sr_{0.075}Ba_{0.025}Yb_{0.1-}$  $Co_4Sb_{12}$  [35]. These two samples have a ZT  $\approx$  1.4; the same result is obtained for R = Sr of the current series. The sample with R = Sr has the lowest lattice thermal conductivity of the series, whereas the lattice thermal conductivities for  $Sr_{0.075}Ba_{0.025}Yb_{0.1}Co_{4}Sb_{12}\ [35]\ and\ Ba_{0.08}La_{0.05}Yb_{0.04}Co_{4}.$ Sb<sub>12</sub> [39] calculated with  $L_0 = 2.45 \times 10^{-8} \text{ W } \Omega \text{ K}^{-2}$  at 820 K yield negative values. Therefore the outstanding high ZT > 1.6 at 820 K reaching ZT = 1.7 at 850 K with a power factor <6 mW cm<sup>-1</sup> K<sup>-1</sup> of Shi et al. [39] is due to the extremely low thermal conductivity.

## 4. Optimization of the TE performance by nanostructuring of set 2

#### 4.1. Sample preparation and structural characterization

For the second part of this work, samples with excess Yb (nominal composition  $(Sr_{0.25}Ba_{0.25}Yb_{0.5})_{0.5}Co_4Sb_{12.5}$ ) and weighing 20 g each were prepared in a way similar to the  $(R_{0.33}Ba_{0.33}Yb_{0.33})_{0.35}Co_4Sb_{12.3}$  samples described above (see Section 2). However, the  $(Sr_{0.25}Ba_{0.25}Yb_{0.5})_{0.5}$ Co<sub>4</sub>Sb<sub>12.3</sub> samples showed a superposition of X-ray powder diffraction maxima from skutterudites of different compositions. In order to homogenize the samples, the material was additionally annealed at 750 for 7 days. Subsequent ball milling for 2 h at 200 rpm (main disc) and -500 rpm

(vessels), and hot pressing for 2 h at 650 °C and 56 MPa resulted in a homogeneous sample, labelled Sr(S), with the skutterudite composition Sr<sub>0.10</sub>Ba<sub>0.12</sub>Yb<sub>0.04</sub>Co<sub>4</sub>Sb<sub>12</sub> and secondary phases, forming microsized grains, as can be seen in the SEM (Fig. 7a) and TEM images (Fig. 7d).

To introduce nanostructuring, the specimen was crushed into particles with sizes below 150  $\mu$ m and subjected to lowenergy ball milling for 14 h at 140 rpm (main disc) and -350 rpm (vessels). XPD of the ball-milled sample showed a significant broadening of the diffraction maxima, indicating nanostructuring of the skutterudite. However, the broadening almost entirely vanished after hot pressing at 700 °C (40 MPa, 2 h) and subsequent annealing for 24 days at 700 °C, indicating that the nanocrystallites of the skutterudite phase coagulated during the heat treatment at the high processing temperatures.

In order to investigate the influence of the grain boundaries and particle size distribution on the TE properties, the sample was once more processed in the following way. One part of the sample was manually ground to grain sizes of 53–70  $\mu m$  after sieving (sample  $Sr_{HM}(B)$ ). The remaining part was ball milled for 14 h at 140 rpm (sample Sr(A)). For two further samples the powders of the ball-milled sample Sr(A) and manually ground sample  $Sr_{HM}(B)$  were mixed in a weight ratio of (i) 80% Sr(A) and 20%  $Sr_{HM}(B)$  (hereinafter called sample Sr(C)) and (ii) 60% Sr(A) and 40%  $Sr_{HM}(B)$  (hereinafter called sample Sr(D)). All four samples were hot pressed for 2 h at 650 °C and 56 MPa.

Characterization of the samples by means of EPMA and XPD (Table 1) showed that the composition of the skutter-udite phase in all five samples (Sr(S), Sr(A), Sr(B), Sr(C) and Sr(D)) was very similar to that obtained for the sample of set 1 with R = Sr discussed in the previous section. We should note that almost no difference was observed in the microstructure of samples Sr(A) and  $Sr_{HM}(B)$  as well as for their mixtures (samples Sr(C) and Sr(D)). XPD peaks indicated ytterbium oxide, and the SEM image of sample Sr(A) showed a homogeneous distribution of white nanoinclusions (Fig. 7b,c). Due to the small grain size of these precipitates we were not able to identify their composition either by EPMA or XPD; however, EPMA of some bigger particles indicated that the precipitations were enriched by ytterbium.

TEM investigations (Fig. 7d) on the samples Sr(S) and Sr(A) revealed in the sample Sr(S) not only YbSb<sub>2</sub> as secondary phase but also Yb<sub>2</sub>O<sub>3</sub> and Sb. The white nanosized inclusions already found in the SEM images of the sample Sr(A) could be identified as Yb<sub>2</sub>O<sub>3</sub>; all of these Yb<sub>2</sub>O<sub>3</sub> precipitations are distributed at the grain boundaries (Fig. 7e).

#### 4.2. Physical properties

Figs. 8–12 show the TE properties of the samples Sr(A),  $Sr_{HM}(B)$ , Sr(C) and Sr(D) in comparison to the original sample Sr(S) and the respective sample from the previous set with R = Sr (set 1) (see Section 3). Note that the compositions of the skutterudites for all specimens are within

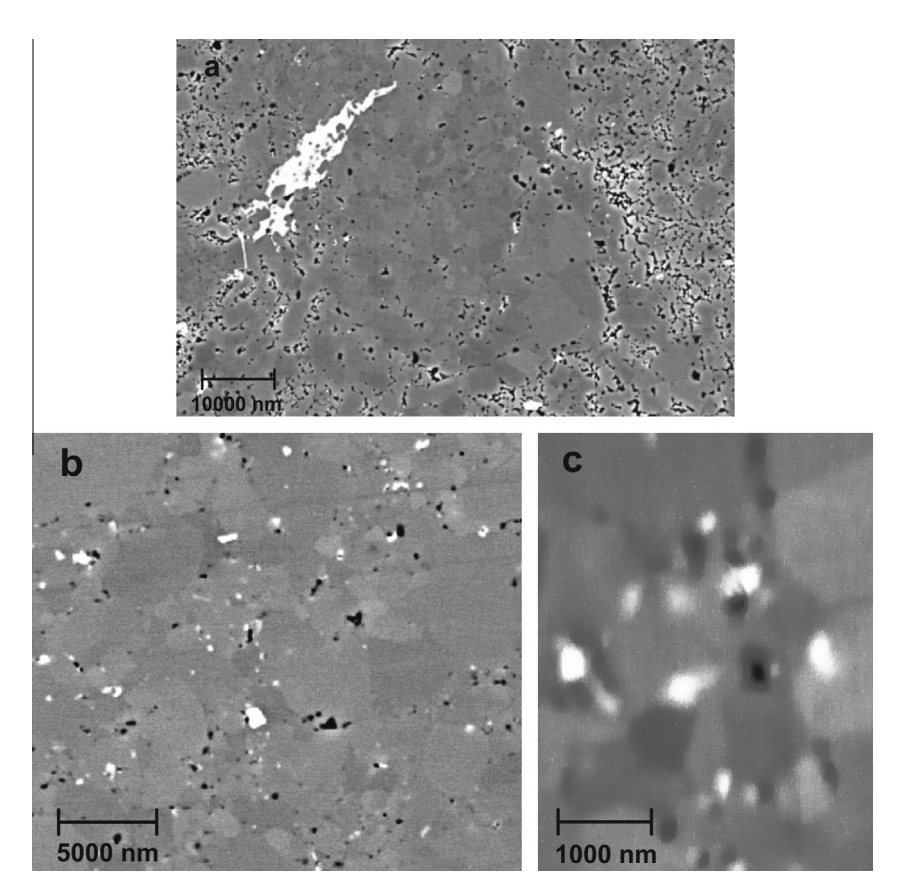


Fig. 7a,b,c. Scanning electron micrograph of the sample with the nominal composition  $(Sr_{0.25}Ba_{0.25}Yb_{0.50})_{0.5}Co_4Sb_{12}$ : (a) original sample (sample Sr(S)) and (b, c) after nanostructuring (sample Sr(A)) showing equally distributed precipitates, and especially the introduced nanoprecipitates (c).

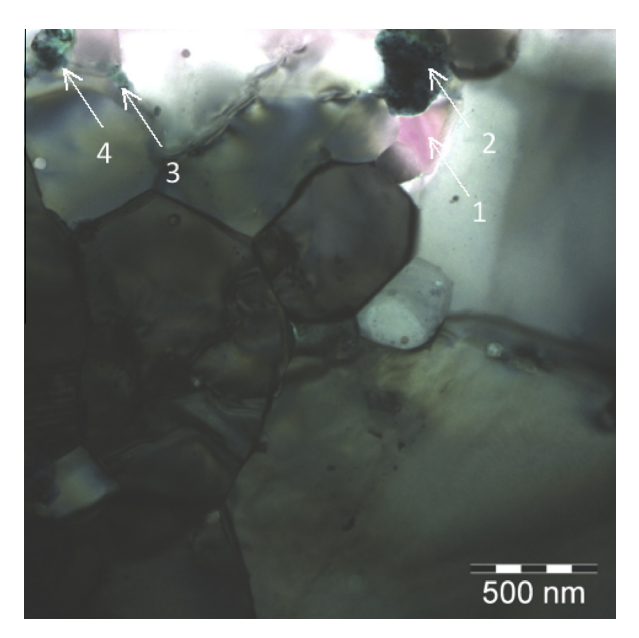


Fig. 7d. Superimposed energy-filtered (17, 31, and 59 eV) TEM image (RGB) of Sr(S). The white arrows indicate secondary phases (1: Sb, 2,4:  $Yb_2O_3$ , 3:  $YbSb_2 + Yb_2O_3$ ).

the measurement error of EPMA and XPD (see Table 1), and therefore we may compare the influence of various parameters on TE properties. Comparing the two samples

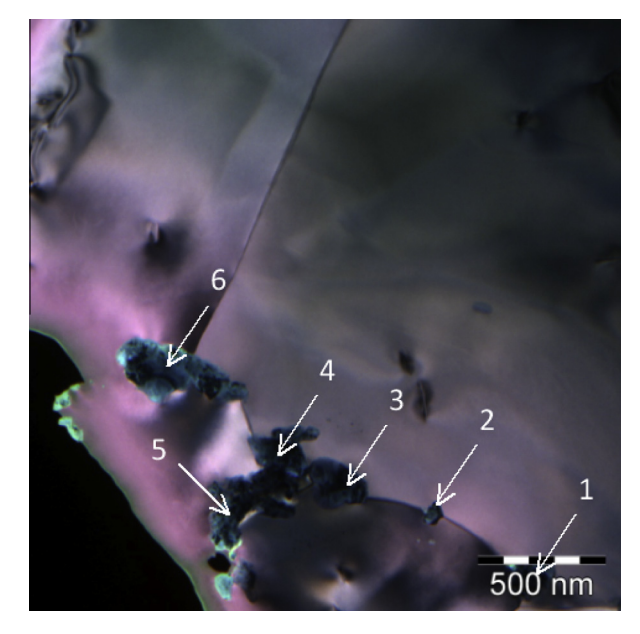


Fig. 7e. Superimposed energy-filtered (17, 31, and 59 eV) TEM image (RGB) of Sr(A). The white arrows indicate nanosized  $Yb_2O_3$  phases.

with the nominal compositions  $(Sr_{0.33}Ba_{0.33}Yb_{0.33})_{0.35}Co_4$ .  $Sb_{12.3}$  (denoted as  $Sr(set\ 1)$ ) and  $(Sr_{0.25}Ba_{0.25}Yb_{0.50})_{0.5}Co_4$ .  $Sb_{12.5}$  (Sr(S)), the influence of the secondary phases  $(Yb_2O_3,\ Sb\ and\ YbSb_2)$  can be seen. By comparing the

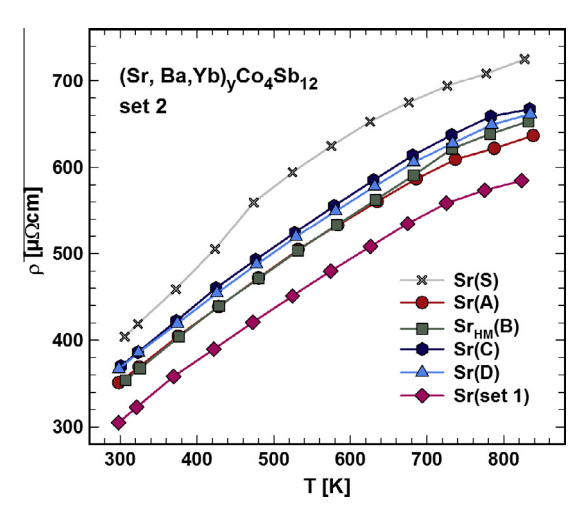


Fig. 8. Samples of set 2: electrical resistivity,  $\rho$ , vs. temperature T of  $(Sr(S,A,B_{HM},C,D),Ba,Yb)_yCo_4Sb_{12}$  in comparison to sample R=Sr of set 1

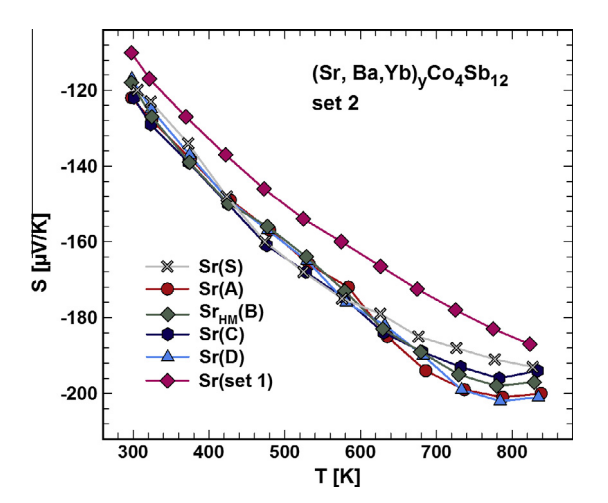


Fig. 9. Samples of set 2: Seebeck coefficient, S, vs. temperature T of  $(Sr(S,A,B_{HM},C,D),Ba,Yb)_yCo_4Sb_{12}$  in comparison to sample R=Sr of set

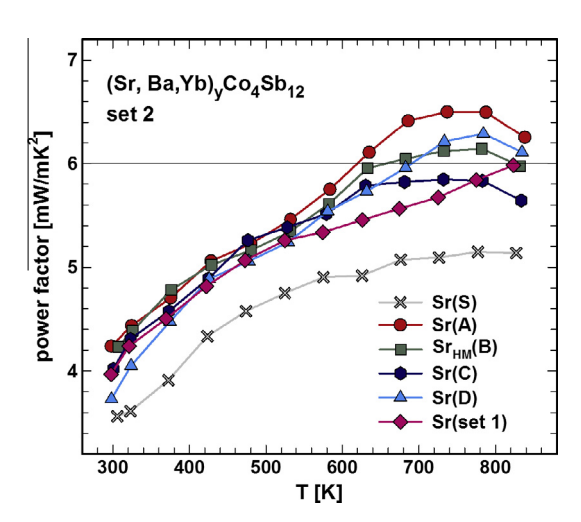


Fig. 10. Samples of set 2: power factor, pf, vs. temperature T of  $(Sr(S,A,B_{HM},C,D),Ba,Yb)_yCo_4Sb_{12}$  in comparison to sample R=Sr of set 1.

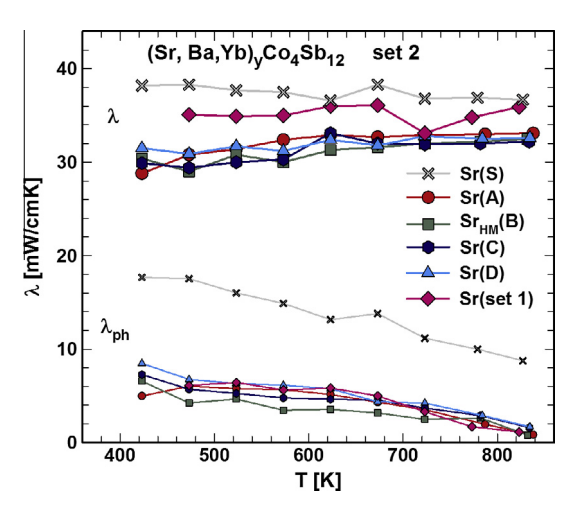


Fig. 11. Samples of set 2: thermal conductivity,  $\lambda$ , and lattice thermal conductivity,  $\lambda_{ph}$ , vs. temperature T of  $(Sr(S,A,B_{HM},C,D),Ba,Yb)_yCo_4Sb_{12}$  in comparison to sample R = Sr of set 1.

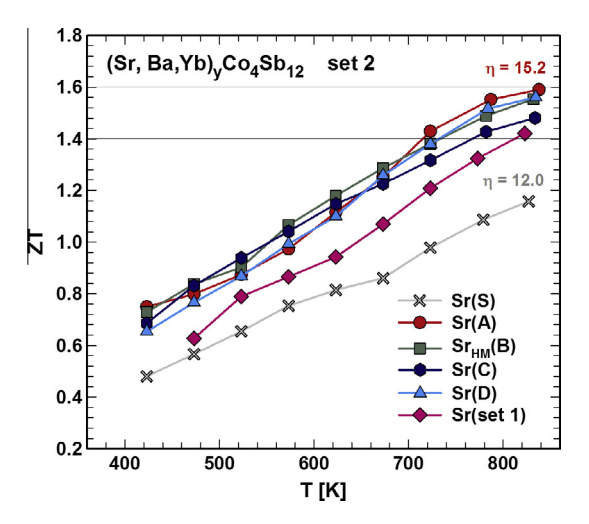


Fig. 12. Samples of set 2: figure of merit, ZT, vs. temperature T of  $(Sr(S,A,B_{HM},C,D),Ba,Yb)_yCo_4Sb_{12}$  in comparison to sample R=Sr of set 1.

TE properties of these two samples with the samples Sr(A–D) containing homogeneously distributed nano-inclusions of the secondary phase (Yb<sub>2</sub>O<sub>3</sub>), the influence of such nanostructuring can be investigated.

Electrical resistivity (Fig. 8) exhibits the behavior of heavily doped semiconductors;  $\rho(T)$  increases with increasing temperature, being independent of the original grain sizes. Microcrystalline Yb<sub>2</sub>O<sub>3</sub> (sample Sr(S)), however, significantly increases the electrical resistivity (about 30%) whereas nanostructuring of the Yb<sub>2</sub>O<sub>3</sub> phase results in a reduction (sample Sr(A)). Despite of this reduction the resistivity is still higher than for the reference sample Sr(set 1).

The absolute values of the negative Seebeck coefficients (Fig. 9) are quite close to each other, and the influence of the impurity phase is not so evident. Again, the sample with the lowest resistivity has the lowest thermopower.

Due to the similar slopes of the temperature dependence of the Seebeck coefficient in the temperature range from 300 to 400 K, the calculated electron carrier densities n are similar for all samples (for details see Table 2). The mobilities, calculated via Eq. (3), are in the range of 25–28 cm<sup>2</sup> V<sup>-1</sup> s<sup>-1</sup>. For the sample Sr(A) the Hall coefficient with  $R_H = -0.00918$  cm<sup>3</sup> C<sup>-1</sup> and the electrical resistivity with  $\rho = 343.4 \,\mu\Omega$  cm were measured at T = 296.2 K, revealing  $n = 6.81 \times 10^{20}$  cm<sup>-3</sup> and  $\mu = 26.72$  cm<sup>2</sup> V<sup>-1</sup> s<sup>-1</sup>. These values are in good agreement with the calculated data  $(n = 6.7 \times 10^{20} \, \text{cm}^{-3}, R_H = -0.01 \, \text{cm}^3 \, \text{C}^{-1}$  and  $\mu = 26.7 \, \text{cm}^2 \, \text{V}^{-1} \, \text{s}^{-1}$ , respectively, for T = 300–400 K and  $\rho = 351 \,\mu\Omega$  cm).

Although the differences in the electrical resistivity and Seebeck coefficient were only small for the samples Sr(A),  $Sr_{HM}(B)$ , Sr(C) and Sr(D), some differences can be distinguished in the power factor curve (Fig. 10) above 600 K, showing relatively and absolutely a maximum value of 6.5 mW m<sup>-1</sup> K<sup>-2</sup> at 750 K for the sample Sr(A). The influence of the impurities, resulting in the lowest power factor values, is obvious as can be seen for sample Sr(S).

Thermal conductivity throughout the temperature range (420 to  $\sim 835 \text{ K}$ ) (Fig. 11) increases slightly with increasing temperature and is in the range of 29–36 mW cm<sup>-1</sup> K<sup>-1</sup> for all samples with exception of sample Sr(S), which has not only higher values but seems to be more or less constant. The lattice thermal conductivity was calculated as described in Section 3.2. In general, the lattice thermal conductivity decreases with increasing temperature. The low data are attributed to the small and mixed grains as well as to the precipitates in these samples; however, it is significantly higher for sample Sr(S) which contains microcrystalline grains.

ZT is shown in Fig. 12 and is increasing almost linearly over the whole temperature range from 420 to 835 K. Sample Sr(D) has ZT > 1.4, and the samples Sr(A), Sr(B) and Sr(C) have ZT values of up to 1.6 (for Sr(A)), which proves that (i) the ZT values of the (Sr,Ba,Yb) $_{y}$ Co $_{4}$ Sb $_{12}$  skutterudites are reproducible, and (ii) that nanoprecipitates positively influence the physical properties and further increase the figure of merit, ZT.

Fig. 6a and b summarize all the TE properties averaged for the temperature range 473-823 K as well as those at 830 K (in some cases extrapolated data). The average values of the physical properties of set 2 (Fig. 6a) show no big differences for the samples Sr(A), Sr(B), Sr(C) and Sr(D), and are also in the same range as for sample R = Sr (set 1); however, Sr(S) not only has a lower average power factor but also a considerably higher thermal and lattice thermal conductivity, resulting in a rather low average ZT value documenting the negative influence of microcrystalline grains. It is also interesting to see that the difference in grain size in set 1 (R = Sr and  $R = Sr_{HM}$ ) was much more pronounced than in set 2. Although sample Sr(A), the pure ball-milled sample, exhibited the best TE performance, resulting in the highest ZT, the three other samples, Sr<sub>HM</sub>(B), Sr(C) and SR(D), show similar good results due to nanoprecipitation and the fact that the difference in grain sizes was negligible.

The thermal–electric conversion efficiency  $\eta$  for the samples of set 2 with exception of sample Sr(S) ( $\eta = 12.0$ ) is higher than for the samples of set 1 because of the higher average ZT values ( $14.9 \le \eta \le 15.2$ ).

### 5. Changes after severe plastic deformation via high-pressure torsion

After HPT deformation sample Sr(A) had a slightly increased lattice parameter (a = 0.90599(4)) (Fig. 13b) and a decreased density ( $d_m = 7.3 \text{ g cm}^{-3}$ ), a behavior common for HPT-treated filled skutterudites [47,54,56,57,62]. The growth of the unit cell dimensions arises due to the enhanced formation of structural defects introduced through HPT. The reason for the lower densities is the appearance of very fine microcracks introduced during severe plastic deformation. After measurement-induced heating (300–823 K within 5 h, during the measurement of the Seebeck coefficient and electrical resistivity) the lattice parameter of the untreated sample Sr(A) is practically the same, whereas the lattice parameter of the HPT-processed sample is decreased, though does not attain its original size. This behavior indicates that defects heal but not completely, a common finding for HPT-processed skutterudites.

Comparing the X-ray patterns before and after HPT, peak broadening is evident for all peaks as can be seen, for example, for the (361) peak (Fig. 13a). This change in the half width is parallel to the change in the lattice parameter, indicating a change in the crystallite size and dislocation density, i.e. the broader the peak, the smaller the crystallite size.

Figs. 14a–d show the changes in the physical properties of sample Sr(A) after HPT processing. The electrical resistivity (Fig. 14a) of the warming-up curve at room temperature is about twice as high as before HPT; it increases with increasing temperature and after a maximum at about 620 K decreases. This behavior was also found for other HPT-processed skutterudites [47,54,56,57,62] as well as for the clathrate Ba<sub>8.00</sub>Cu<sub>3.66</sub>Ge<sub>40.30</sub>In<sub>1.65</sub> [63]. The behavior indicates that the grains start to grow and/or fine cracks fuse together. For the measurement with decreasing temperature the electrical resistivity curve indicates metallic behavior, although the values are still higher than before HPT because not all defects are annealed out. The changing sizes of the lattice parameter confirm this behavior (Fig. 13). The lattice parameter, which increased after

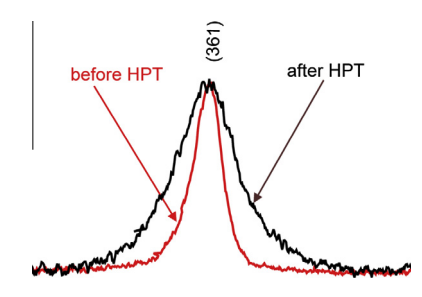


Fig. 13a. X-ray profile of Sr(A) before and after HPT processing.

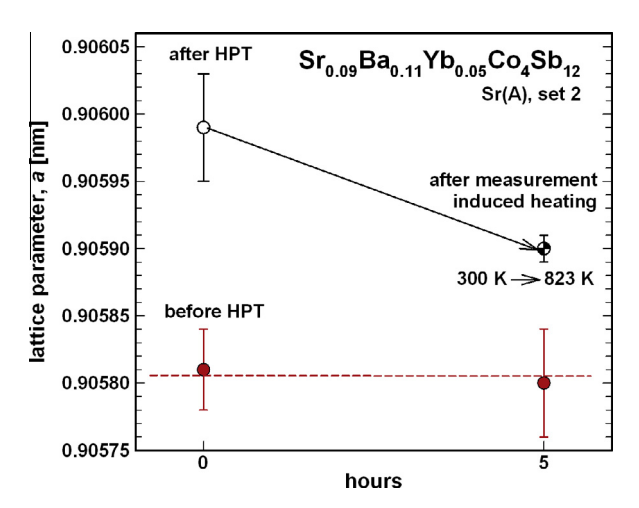


Fig. 13b. Lattice parameter, a, vs. annealing time in hours for Sr(A) before and after HPT processing and after measurement-induced heating.

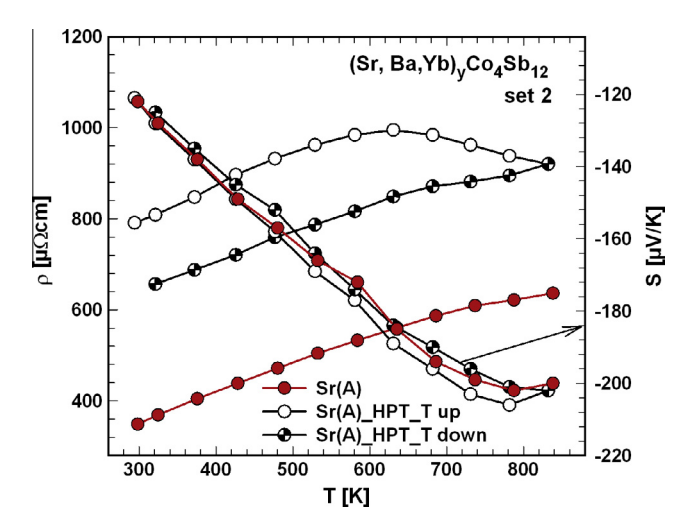


Fig. 14a. Electrical resistivity and Seebeck coefficient vs. temperature of sample Sr(A) of set 2 before and after HPT processing.

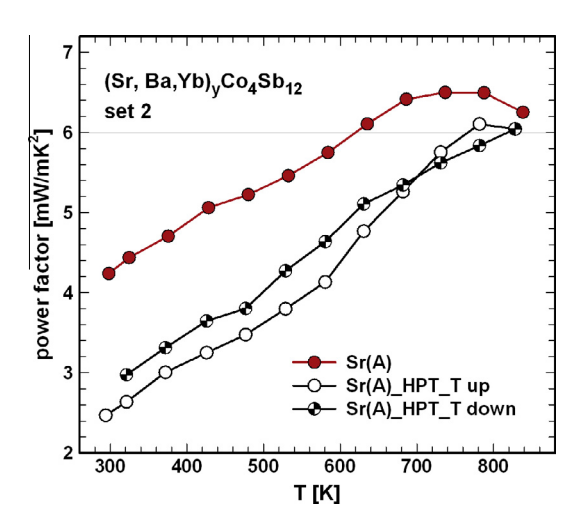


Fig. 14b. Power factor vs. temperature of sample Sr(A) of set 2 before and after HPT processing.

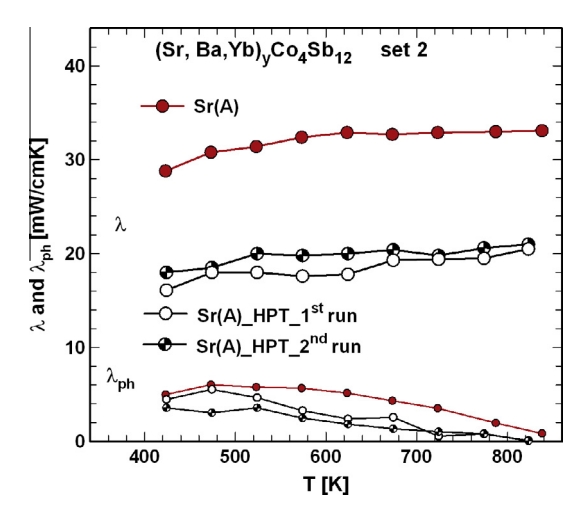


Fig. 14c. Thermal conductivity and lattice thermal conductivity vs. temperature of sample Sr(A) of set 2 before and after HPT processing.

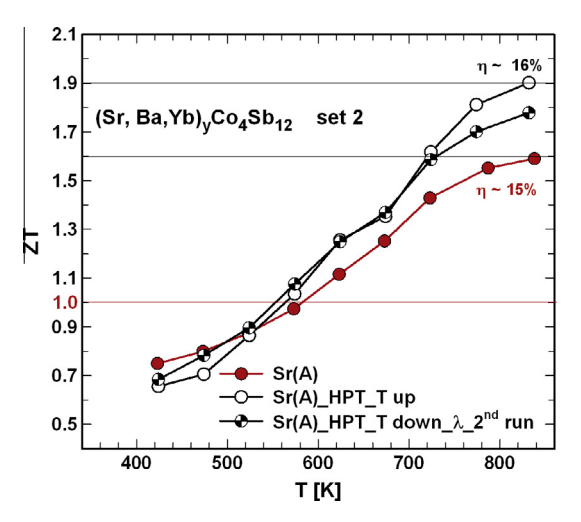


Fig. 14d. ZT vs. temperature of sample Sr(A) of set 2 before and after HPT processing.

HPT processing, is decreased not to its original size but to a = 0.90590(1), indicating that after the measurement-induced heating (i) defects have only partly annealed out and (ii) many cracks have fused together due to grain growth. It is well known from our previous studies [47,54,56,57,62] that the resistivity curve determined from third and fourth measurements is practically identical to that of the cooling-down curve, which means that once defects are reduced and most of the cracks are fused together, the material is stable with respect to temperature changes. Moreover, the lattice parameter does not change afterwards any further.

The Seebeck coefficient (Fig. 14a) does not differ significantly from the one before HPT. The crystallite size is smaller after HPT (~40 nm) but not small enough to positively influence the thermopower. The slopes of the Seebeck coefficients before and after HPT processing are similar (Fig. 14a), and therefore the calculated values of the charge carrier densities (using Eq. (1)) are also similar

with  $n=6.4\times10^{20}~\rm cm^{-3}$  for the measurement immediately after HPT processing and  $n=6.5\times10^{20}~\rm cm^{-3}$  after measurement-induced heating. As the lattice parameter and therefore also the cell volume are enlarged after HPT processing, but the number of electrons is constant, then as a consequence n becomes smaller. The data for n are also consistent with respect to the higher electrical resistivity values after HPT. The mobilities (Eq. (3)) with  $\mu\approx12~\rm cm^2~V^{-1}~s^{-1}$  and  $\mu\approx15~\rm cm^2~V^{-1}~s^{-1}$  are lower than before HPT, indicating a change in the scattering mechanism of the electrons.

The power factor (Fig. 13b) increases almost linearly with increasing temperature; however, the power factor is lower after HPT processing due to the high electrical resistivity. Additionally the power factor has a much steeper rise for the deformed skutterudite and above 760 K it reaches almost the values of the untreated sample.

Whereas the introduced defects, the increased dislocation density and fine cracks are detrimental to the electrical resistivity, they are advantageous for the thermal conductivity (Fig. 14c), lowering the values by about 40% with respect to those before HPT processing. A second measurement of the thermal conductivity showed almost the same result as the first one. The lattice thermal conductivity is only slightly lower than before HPT and decreases with decreasing temperature.

The figure of merit ZT (Fig. 14d) below 580 K is in the same range as before HPT but above 580 K ZT is higher, resulting in ZT = 1.9 at 835 K for the first measurement with rising measuring temperature: this is an enhancement of about 20% in comparison to the value before HPT. As the measurement with decreasing temperature and the second measurement of the thermal conductivity can be regarded as reproducible, a stable ZT = 1.8 yields an enhancement of almost 13%. The thermal–electric conversion efficiency  $\eta$  has increased after HPT to  $\eta = 16\%$ .

#### 6. Conclusions

Bulk n-type triple- and multifilled skutterudites with the composition  $(R_{0.33}Ba_{0.33}Yb_{0.33})_{0.35}Co_4Sb_{12.3}$ (R = Sr, La, DD, MM, SrMm, SrDD) have been synthesized by combining a melting reaction technique with ball milling or grinding by hand and hot pressing. Structural and physical properties have been investigated - the latter in the temperature range from 300 to 823 K – and have been compared with the results from earlier studies by the authors [35,37] and reported in the literature [39]. Power factors were found to increase with fillers DD, Mm, La, Sr, reaching an extraordinarily high value of 6 mW cm<sup>-1</sup> K<sup>-1</sup> for Sr at 823 K. For skutterudites with R = SrMm and SrDD the power factor is between those of R = Sr and Mm and R = Sr and DD, respectively. The lattice thermal conductivity in this series decreases in the same sequence. The same sequence appears consistently when comparing the ZT values with a well reproducible maximum value for the triple-filled skutterudite with  $R = Sr \text{ with } ZT \approx 1.4 \text{ at } 823 \text{ K}.$ 

It could be demonstrated that YbSb<sub>2</sub>, Sb and Yb<sub>2</sub>O<sub>3</sub> as secondary phases reduced the TE performance due to a decreased power factor and an increased lattice thermal conductivity. However, a homogeneous and nanoscale distribution of Yb<sub>2</sub>O<sub>3</sub> impurities improves the TE performance significantly, resulting finally in ZT values of  $\sim$ 1.6 at 835 K for R = Sr(A) (Sr<sub>0.09</sub>Ba<sub>0.11</sub>Yb<sub>0.05</sub>Co<sub>4</sub>Sb<sub>12</sub>).

The sample with R = Sr(A),  $Sr_{0.09}Ba_{0.11}Yb_{0.05}Co_4Sb_{12}$ , was additionally processed by HPT. Although the electrical resistivity was enhanced and the Seebeck coefficient remained the same, an extremely low thermal conductivity yielded a 20% higher ZT, resulting in ZT = 1.9 at 835 K for the first measurement (warming up), approaching a stable value, ZT = 1.8, on further temperature cycling.

#### References

- [1] Rowe DM. Handbook of thermoelectrics. Boca Raton (FL): CRC Press; 2006.
- [2] Jeitschko W, Braun DJ. Acta Crystallogr B 1977;33:3401.
- [3] Hicks L, Dresselhaus M. Phys Rev B 1993;47:16631.
- [4] Meisner GP, Morelli DT, Hu S, Yang J, Uher C. Phys Rev Lett 1998:80:3551.
- [5] Venkatasubramanian R, Siivola E, Colpitts T, O'Quinn B. Nature 2001;413:597.
- [6] Chen LD, Kawahara T, Tang XF, Goto T, Hirai T, Dyck JS, et al. J Appl Phys 2001;90(4):1864.
- [7] Chen G, Shakouri A. J Heat Transfer 2002;124:242.
- [8] Nolas GS, Fowler G, Yang J. J Appl Phys 2006;100(4). 43705-1-4.
- [9] Morelli DT, Meisner GP. J Appl Phys 1995;77(8):3777.
- [10] Morelli DT, Caillat T, Fleurial JP, Borshchevsky A, Vandersande J, Chen B, et al. Phys Rev B 1995;51(15):9624.
- [11] Pei YZ, Chen LD, Zhang W, Shi X, Bai SQ, Zhao XY, et al. Appl Phys Lett 2006;89:221107.
- [12] Morelli DT, Meissner GP, Chen B, Hu S, Uher C. Phys Rev B 1997;56(12):7376.
- [13] Keppens V, Mandrus D, Sales BC, Chakoumakos BC, Dai P, Coldea R, et al. Nature 1998;395:876.
- [14] Nolas GS, Cohn JL, Slack GA. Phys Rev B 1998;58:164.
- [15] Nolas GS, Kaeser M, Littleton IV RT, Tritt TM. Appl Phys Lett 2000;77:1855.
- [16] Lamberton Jr GA, Bhattacharya S, Littleton IV RT, Kaeser MA, Tedstrom RH, Tritt TM, et al. Appl Phys Lett 2002;80(4):598.
- [17] Hermann RP, Jin R, Schweika W, Grandjean F, Mandrus D, Sales BC, et al. Phys Rev Lett 2003;90(13):135505.
- [18] Kuznetsov VL, Kutznetsova LA, Rowe DM. J Phys: Condens Matter 2003;15:5035.
- [19] Puyet M, Lenoir B, Dauscher A, Dehmas M, Stiewe C, Müller E. J Appl Phys 2004;95(9):4852.
- [20] Zhao XY, Shi X, Chen LD, Zhang WQ, Zhang WB, Pei YZ. J Appl Phys 2006;99:053711.
- [21] Pei YZ, Yang J, Chen LD, Zhang W, Salvador JR, Yang J. Appl Phys Lett 2009;95:042101.
- [22] Pei YZ, Yang J, Chen LD, Bai SQ, Zhao XY, Li XY. Scripta Mater 2007;56:621.
- [23] Yang J, Zhang W, Bai SQ, Mei Z, Chen LD. Appl Phys Lett 2007;90:192111.
- [24] Shi X, Kong H, Li CP, Uher C, Yang J, Salvador JR, et al. Appl Phys Lett 2008;92:182101.
- [25] Uher C, Shi X, Kong H. Mater Res Soc Symp Proc 2008;1044-U05-09
- [26] Bai SQ, Pei YZ, Chen LD, Zhang WQ, Zhao XY, Yang J. Acta Mater 2009;57:3135.
- [27] Zhao W, Wei P, Zhang Q, Dong C, Liu L, Tang X. J Am Chem Soc 2009;131:3713.

- [28] Li H, Tang X, Zhang Q, Uher C. Appl Phys Lett 2009;94:102114.
- [29] Li D, Yang K, Hng HH, Yan QY, Ma J, Zhu TJ, et al. J Phys D: Appl Phys 2009;42:105408.
- [30] Fukuoka H, Yamanaka S. Chem Mater 2010;22:47.
- [31] Salvador JR, Yang J, Wang H, Shi X. J Appl Phys 2010;107:043705.
- [32] Bai SQ, Huang XY, Chen LD, Zhang W. Appl Phys A 2010;100:1109.
- [33] Rogl G, Grytsiv A, Rogl P, Bauer E, Zehetbauer M. Intermetallics 2011;19:546.
- [34] Rogl G, Grytsiv A, Rogl P, Bauer E, Kerber MB, Zehetbauer M, et al. Intermetallics 2010:18:2435.
- [35] Zhang L, Grytsiv A, Rogl P, Bauer E, Zehetbauer M. J Phys D: Appl Phys 2009;42:225405.
- [36] Zhang L, Melnychenko-Koblyuk N, Royanian E, Grytsiv A, Rogl P, Bauer E. J Alloys Compd 2010;504:53.
- [37] Rogl G, Grytsiv A, Melnychenko-Koblyuk N, Bauer E, Laumann S, Rogl P. J Phys: Condens Matter 2011;23:275601.
- [38] Shi X, Salvador JR, Yang J, Wang H. J Electron Mater 2009;38(7):930.
- [39] Shi X, Yang J, Salvador JR, Chi M, Cho JY, Wang H, et al. J Am Chem Soc 2011;133:7837.
- [40] Yang J, Morelli DT, Meisner GP, Chen W, Dyck JS, Uher C. Phys Rev B 2003;67:165207.
- [41] Ballikaya S, Wang G, Sun K, Uher C. J Electron Mater 2011;40:570.
- [42] Zehetbauer M, Seumer V. Acta Metall Mater 1993;41:57.
- [43] Zehetbauer M, Stüwe HP, Vorhauer A, Schafler E, Kohout J. Adv Eng Mater 2003;5:33.
- [44] Zehetbauer M, Kohout J, Schafler E, Sachslehner F, Dubravina A. J Alloys Compd 2004;378:329.
- [45] Müller M, Zehetbauer M, Borbely A, Ungar T. Scripta Mater 1996;35:146.
- [46] Ungar T, Zehetbauer M. Scripta Mater 1996;35:146.
- [47] Zhang L, Grytsiv A, Bonarski B, Kerber M, Setman D, Schafler E, et al. J Alloys Compd 2010;494:78.

- [48] Ashida M, Hamachiyo T, Hasezaki K, Matsunoshita H, Kai M, Horita Z. Mater Sci Forum 2008;584–586:1006.
- [49] Ashida M, Hamachiyo T, Hasezaki K, Matsunoshita H, Kai M, Horita Z. J Phys Chem Solids 2009;70:1089.
- [50] Sun ZM, Hashimoto H, Keawprak N, Ma AB, Li LF, Barsoum MW. J Mater Res 2005;20(4):895.
- [51] Wacha W. Program STRUKTUR. Diploma thesis, University of Technology, Vienna; 1989.
- [52] Rodriguez-Carvajal JJ. FULLPROF, A program for Rietveld refinement and pattern matching analysis. Abstract of the satellite meeting on powder diffraction of the XV congress. Int. Union of Crystallography, Talence, France; 1990, p. 127.
- [53] Eyidi D, Eibl O. Micron 2002;33:499.
- [54] Rogl G, Aabdin Z, Schafler E, Horky J, Setman D, Zehetbauer M, et al. J Alloys Compd 2012;537:183–9.
- [55] Rogl G, Grytsiv A, Royanian E, Heinrich P, Bauer E, Rogl P, et al. J Alloys Compd 2012;537:242.
- [56] Rogl G, Zehetbauer M, Kerber M, Rogl P, Bauer E. Mater Sci Forum 2011;667–669:1089–94.
- [57] Rogl G, Setman D, Schafler E, Horky J, Kerber M, Zehetbauer M, et al. Acta Mater 2012;60:2146.
- [58] Vorhauer A, Pippan R. Scripta Mater 2004;51:921.
- [59] Rogl G, Zehetbauer M, Kerber M, Rogl P, Bauer E. Mater Sci Forum 2011;667–669:1089.
- [60] Zhang L, Grytsiv A, Kerber M, Rogl P, Bauer E, Zehetbauer M, et al. J Alloys Compd 2009;481:106.
- [61] Cahill D, Pohl R. Solid State Commun 1989;70(10):927.
- [62] Rogl G, Rogl P, Bauer E, Zehetbauer M. Severe plastic deformation, a tool to enhance thermoelectric performance. In: Mori T, Koumoto K, editors. Thermoelectric nanomaterials. Berlin: Springer Verlag; 2013.
- [63] Yan X, Falmbigl M, Rogl G, Grytsiv A, Prokofiev A, Bauer E, et al. J Electron Mater 2013;42(7):1330.